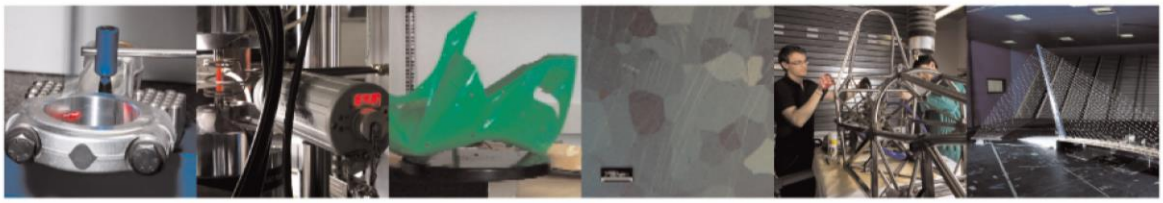

Micro laser metal wire deposition of thin-walled Al alloy components: Process and material characterization

Demir, Ali Gökhan; Biffi, Carlo Alberto

This is a post-peer-review, pre-copyedit version of an article published in JOURNAL OF MANUFACTURING PROCESSES. The final authenticated version is available online at: http://dx.doi.org/10.1016/j.jmapro.2018.11.017

DIPARTIMENTO DI MECCANICA ■ POLITECNICO DI MILANO
via G. La Masa, 1 ■ 20156 Milano ■ EMAIL (PEC): pecmecc@cert.polimi.it
http://www.mecc.polimi.it
Rev. 0

Micro laser metal wire deposition of thin-walled Al alloy components: process and material characterization

Ali Gökhan Demir[1], Carlo Alberto Biffi[2]

[1]Department of Mechanical Engineering, Politecnico di Milano, Via La Masa 1, 20156 Milan, Italy

[2]National Research Council, CNR ICMATE, Institute of Condensed Matter Chemistry and Technologies for Energy; Via Previati 1, 23900 Lecco, Italy.

*Corresponding author; aligokhan.demir@polimi.it

Micro laser metal wire deposition of thin-walled Al alloy components: process and material characterization

Ali Gökhan Demir[1], Carlo Alberto Biffi[2]

[1]Department of Mechanical Engineering, Politecnico di Milano, Via La Masa 1, 20156 Milan, Italy

[2]National Research Council, CNR ICMATE, Institute of Condensed Matter Chemistry and Technologies for Energy, Via Previati 1, 23900 Lecco, Italy.

*Corresponding author; aligokhan.demir@polimi.it

Abstract

In this work, micro laser metal wire deposition (μLMWD) of 0.4 mm diameter 4047 Al-alloy (AlSi12) wire is demonstrated. A flash-pumped Nd:YAG laser producing ms-long pulses was used as the energy source. The processing conditions were studied for single and multiple-layered tracks, seeking stable deposition conditions. Microhardness, microstructure and chemical composition were analysed. The results showed that thin walls with sub-mm thickness free of pores and cracks could be obtained using the μLMWD process. The material was characterized by a homogenous microhardness profile over the build direction with high values (approximately 120 HV). The improved mechanical properties were due to the redistribution of the Si in form of a micrometric network in the Al-matrix along the deposit. The process was found to be a promising option for producing freestanding components, as well as adding features to existing parts with tailored properties, especially for lightweight applications.

Keywords: Additive manufacturing; AlSi12; micro components; material microstructure; directed energy deposition

1. Introduction

The use of lightweight Ti- and Al-alloys has been widely explored in selective laser melting (SLM) and electron beam melting (EBM) powder bed fusion processes. These processes are characterized by high geometrical precision, ability to produce internal channels, as well as lattice structures [1–3]. Here, Al-alloys show great promise due to their low cost and compositional variety to achieve the desired mechanical properties. However, they are characterised by low processability by lasers due to their high reflectivity and high thermal diffusivity [4]. Not all compositions are usable due to low weldability and crack susceptibility

during the process. On the other hand, the use of Al-alloys with EBM is very difficult due to the low vaporization point of these materials under vacuum.

On the contrary, the use of lightweight metals, especially Al-alloys, in directed energy deposition (DED) processes has been sparingly explored [5–10]. Laser metal deposition (LMD) is the most widely studied DED process, which combines powder feedstock with the laser beam as the energy source [11]. The powder feedstock is blown through coaxial or multi-jet process nozzle to the workspace and is melted by the laser beam. The process is commonly carried out in ambient atmosphere with the use of a shielding gas. Therefore, the use of highly reactive Ti- and Al- alloy powders can be problematic both in terms of safety [12]. The high surface to volume ratio of the metallic powders combined with the reactivity of these materials generate highly explosive conditions around the processing zone. For Al-alloys the high reflectivity remains an important issue as well as the susceptibility to balling due to high surface tension and oxidation [13], and porosity due to gas entrapment [14]. The use of wire feedstock in the same process corresponds to laser metal wire deposition (LMWD), and it is intrinsically safer compared to powder. Additionally to this, the market can offer a large variety of wires in different diameters and different alloy compositions. High purity Al, as well as 4xxx and 5xxx alloy series, and cast alloys such as A356 are available in the market used for welding automotive components, bicycle frames, and marine parts [15,16]. The process is characterized by a higher material usage efficiency [17]. The use of laser as the energy source provides a more precise management of the energy input compared to the use of plasma or arcs [18–20]. The achieved surface finish is comparable to that of the powder based DED processes [21]. However, several limitations exist in the LMWD process. The systems are commonly equipped with lateral wire feeding [22], which generates an asymmetric tool. The deposition trajectories are limited due to this fact. The process lends itself to high deposition rates, reducing the possibility to reach high precision required by many applications [23–25]. Recently, micro laser metal wire deposition (μLMWD) process has been demonstrated [26]. The use of pulsed wave (PW) laser emission with thin wires was proven to be effective in improving dimensional precision to the range of powder-bed fusion techniques. Such geometrical characteristics render the μLMWD process fit best for small components or features that do not require high productivity. Compared to other powder based micro-additive manufacturing processes the process lends itself to thin-walled components rather than complex lattice-like structures [27,28].

Al-alloys have been previously deposited using arcs and electron beam as the energy source [29–32]. However, despite their common use as a filler material in laser welding [33] and these apparent advantages, to the authors' knowledge LMWD of Al-alloy wires have not been treated in the literature.

Accordingly, this paper provides a fundamental study of the μLMWD of thin 4047 Al-alloy wires for producing thin-walled components. In this exploratory work, the process feasibility is sought at first studying single and multiple-layered depositions. In the stable deposition conditions, the material properties are investigated concerning the microstructure, chemical composition variations and microhardness profile. The results are assessed to identify the possibilities to tailor the microstructure of the deposited free-standing parts or added features to existing components.

2. Materials and methods

2.1. Materials

Annealed aluminium 4047 (AlSi12) alloy wire, 0.4 mm in diameter, was used throughout the study together with 5 mm-thick 5754 (AlMg3) base plate. The 4047 alloy, whose chemical composition is reported in Table 1, is at the bordering area of the eutectic composition and is commonly used as filler material in welding and brazing operations Al-alloy castings [34]. The high Si content provides fluidity during the welding process. The base plate alloy is characterized by good weldability. None of the alloys is not heat treatable and material strength mainly relies on the work hardening.

Table 1. Nominal chemical composition of the wire and base plate materials [34]**.**

wt%	Si	Fe	Cu	Ti	Zn	Mn	Mg	Ni	Others	Al
AA 4047	11-13	<0.6	<0.3	<0.15	<0.2	<0.15	<0.1	<0.05	<0.15	Bal.
AA 5754	<0.4	<0.4	<0.1	<0.15	<0.2	<0.5	2.5-4	-	<0.05	Bal.

2.2. μLMWD system

The μLMWD system was based on a custom build wire feeding system, namely Lachesis, and an automated laser welding station (Powerweld HL 124P from Trumpf, Ditzingen, Germany). The laser source mounted on the welding station was a pulsed wave Nd:YAG with 120 W maximum average power. The laser source could be regulated to change the pulse duration (τ) in μs to ms regime and pulse repetition rate (PRR) in Hz order. The maximum pulse energy (E) and the maximum peak power (P_{peak}) were of 50 J and 5 kW, respectively.

The optical chain is composed of fiber delivery with 0.4 mm core diameter, 200 mm collimating and 150 mm focal lenses producing a minimum spot diameter of 0.3 mm. The optical chain can be automatically adjusted to vary the spot diameter between 0.3 and 5 mm. Workpiece positioning could be achieved via 2 linear and a rotational axis, while the process head was mounted on a third linear axis. The transversal speed (v) is controlled through the numerical control of the system. The wire feeder system was controlled through a Labview interface, regulating the wire feed rate (WFR) and synchronising the laser emission at the start of each new layer. The custom-made wire feeding system was mounted on the laser head, allowing to maintain a fixed distance and spot size on the wire. Wire feed direction and wire feeding angle were set manually by setting the position of the wire feeder with respect to the base plate and deposition direction. A shielding gas nozzle was placed to protect the processing zone from oxidation. Laser pulse energy (E), pulse duration and pulse repetition rate were regulated to manage the heat input.

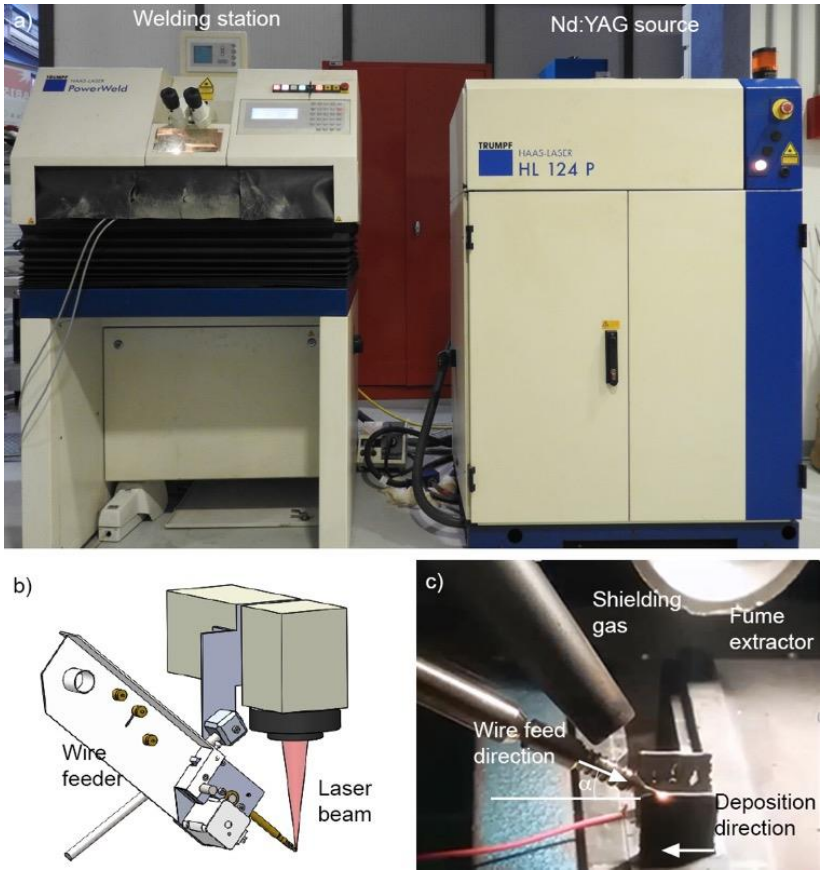

Figure 1. Details of the µWLMD system. a) Overview of the welding station and the laser source. b) CAD model of Lachesis wire feeder. c) Close up image of the deposition zone showing the wire feed and deposition direction.

2.3. Sample characterization

Cross-sections of single-layer deposits and multi-layer thin walls were made by abrasive saw cutting and abrasive paper polishing. Samples were later etched to reveal microstructure with Keller solution. These were observed through optical microscopy (Leitz Ergolux 200 from Leica, Wetzlar, Germany).

Scanning electronic microscopy (SEM) was performed to study microstructure and chemical composition of multi-layered deposition and compared with the ones of the initial wire. This analysis was carried out by means of SEM (LEO 1413 from Zeiss, Oberocken, Germany), equipped with an EDX probe. Finally, mechanical properties of all the samples were evaluated by Vickers micro hardness, using a hardness tester (VMHT 30A from Leica, Wetzlar, Germany), applying a 100 g load for 15 s.

2.4. Experimental plan

The experimental study consisted of two phases for single and multiple layer depositions. After preliminary tests, not reported here for brevity, pulse repetition rate (*PRR*), wire feeding angle (α) and direction, wire feed rate (*WFR*) were fixed at suitable levels allowing for a stable process. Spot diameter (d_s) was chosen 50% larger than the wire diameter at 0.6 mm in order to allow for a complete coverage of the wire without lowering the energy density too much. A relatively slow transverse speed (v) at 70 mm/s was chosen to maintain wire stability. Both pulse energy (E) and pulse duration (τ) were varied in a predetermined feasibility range. A 2_2 factorial plan with central points were executed to determine the conditions providing the smallest deposition width (w). Corner points were replicated twice, whereas 5 replications were produced for the central point. Track length was 10 mm for all experiments. Analysis of variance (ANOVA) was applied to investigate the statistical significance of the parameters. Details of the experimental plan in single-layer deposition study is summarized in Table 2.

In the second phase, multiple layer deposition was studied with the chosen parameter combinations providing the smallest width in a single layer deposition. The aim of this phase was to examine the parameter combinations providing stable depositions for producing thin-walls. As a matter of fact, the height increment is a crucial parameter, which requires to be set correctly to follow the deposition rate of the process [26]. The height increment between consecutive layers (Δz) was tested in a range between 85% and 95% of the average height obtained in the single layer deposition for the chosen parameter set. The resultant range was 210 and

230 μm. Multiple layer depositions with 7, 14, and 21 layers were executed. A 3_2 factorial plan was executed with two replications. In this work, no active control scheme was applied to control the workpiece temperature between layers. Moreover, no interlayer delay has been applied in the experiments to passively control the heat build up. The time between consecutive layers was given by the time required to move the wire feeder to the initial deposition point of the new layer, which was approximately 3 seconds. The results are analysed initially for determining the process feasibility window characterised by a stable process and defect-free deposits. For the stable processing conditions, cross-sections of the produced thin-wall structures were observed through optical microscopy to measure the deposit height. The parameters used in the multi-layer deposition study are summarized in Table 3.

Table 2. Fixed and varied parameters in the study of single-layer depositions experiments.

Fixed parameters	**Level**		
Spot diameter, d_s (mm)	0.6		
Pulse repetition rate, PRR (Hz)	4		
Wire feeding angle, α (°)	30		
Wire feeding direction	Front		
Wire feed rate, WFR (mm/min)	86		
Transverse speed, v (mm/min)	70		
Shielding gas	Ar at 0.5 bar		
Varied parameters	**Levels**		
	Low	Mid	High
Pulse duration, τ (ms)	6	6.5	7
Pulse energy, E (J)	12	12.5	13

Table 3. Fixed and varied parameters in the study of multi-layer depositions experiments.

Fixed parameters	**Level**		
Spot diameter, d_s (mm)	0.6		
Pulse repetition rate, PRR (Hz)	4		
Wire feeding angle, α (°)	30		
Wire feeding direction	Front		
Wire feed rate, WFR (mm/min)	86		
Transverse speed, v (mm/min)	70		
Shielding gas	Ar at 0.5 bar		
Pulse duration, τ (ms)	7		
Pulse energy, E (J)	12		
Varied parameters	**Levels**		
	Low	Mid	High
Height increment, Δz (μm)	210	220	230
Number of layers, N	7	14	21

3. Results

3.1. Single-layer deposition

Figure 2 reports cross-section images of the obtained single-layer deposits as a function of the used process parameters. The images show that the penetration into the base material is limited and the process is based on the welding of the wire material on a conduction mode. A decrease of the deposit width is visible as the pulse duration increases, whereas the influence of the energy level appears limited compared to the pulse duration. Figure 3 shows the width measurements as a function of process parameters. The plot depicts that the influence of pulse duration is stronger, whereas an interaction between the parameters is not expected. The increase of pulse duration from 6 ms to 7 ms results in an average decrease of width from 1050 μm to 850 μm. The observations are confirmed by the analysis of variance, as depicted in Table 4. The only significant factor is the pulse duration with a p-value at 0.001. The decrease in the width as a function of pulse duration can be attribute to the decay of the pulse peak power. At the same levels of energy, the peak power increases as the pulse duration decreases, which can result in a larger melt pool. Overall, the results show that it is feasible to remain in a sub-mm dimensional range, despite the very narrow processing window. The smallest widths observed in the campaign are approximately twice the wire diameter. Out of the experimented region, process instability was observed due to incomplete fusion and balling phenomenon. Accordingly, a further reduction of deposition thickness can be potentially achieved via the reduction of the wire size.

For further processing with multiple-layer deposition, pulse duration was set at 7 ms, as it provided the smallest width conditions. Pulse energy was conveniently chosen at 12 J. Larger energy values were experimentally observed to generate excessive heat build-up during the multiple-layer production.

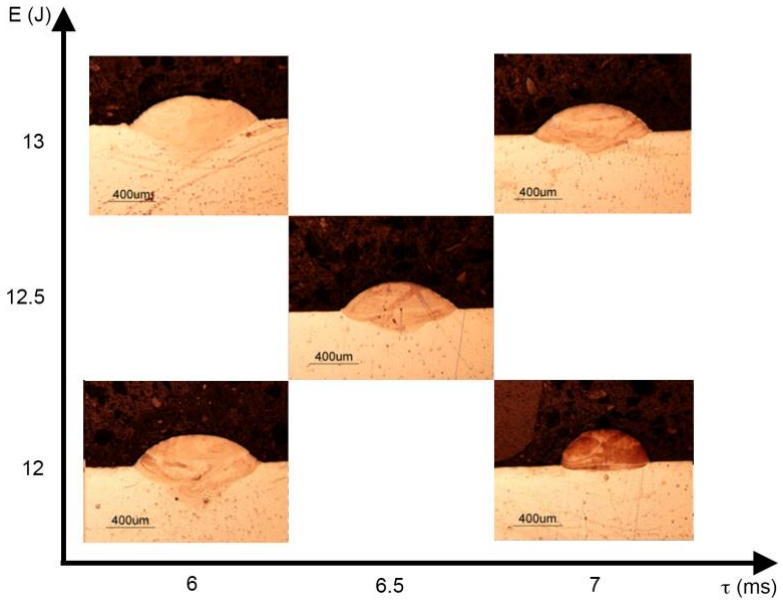

Figure 2. Cross-section images of the single-layer depositions as function of process parameters.

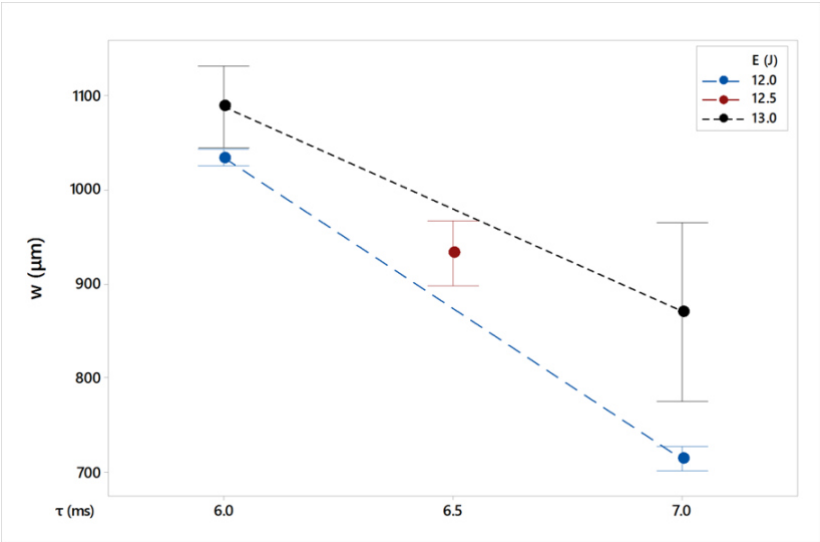

Figure 3. Single track width (*w*) as a function of pulse duration (*τ*) and energy (*E*). Error bars represent standard error.

Table 4. ANOVA table for single track width (w).

Source	DF	Adj SS	Adj MS	F-Value	P-Value
Model	4	172473	43118	7.31	0.009
Linear	2	167212	83606	14.18	0.002
Pulse energy, E (J)	1	22394	22394	3.80	0.087
Pulse duration, τ (ms)	1	144819	144819	24.56	0.001
2-way interactions	1	5160	5160	0.88	0.377
E*τ	1	5160	5160	0.88	0.355
Curvature	1	100	100	0.02	0.899
Error	8	47167	5896		
Total	12	219640			
S= 76.8	R_2=78.53%		R_{2adj}=67.79%		

3.2. Multi-layer deposition and thin wall manufacturing

Figure 4 shows a multiple layered wall successfully built with the μLMWD process. The thin-walled structure is free of defects and the geometry is well defined. Figure 5 depicts the cross-section images of the thin-walled structures obtained in different process parameter combinations. As it can be viewed, the height increment at 230 μm (approximately 95% of the single-layer height) was not suitable for producing structures up to 21 layers. Figure 6 shows the height measurements of the thin-walled structures as a function of layer number and height increment. It can be seen that a linear increase as a function of layer number is present, which does not depend on the height increment. However, an incorrect choice of height increment as in the case of 230 μm results in the failure of the component due to a mismatch between the actual height increase of the component and the commanded height increase of the wire feeder. After 14 layers of deposition, the difference between the height of the deposited material and the wire feeder is approximately 375 μm, a value close the wire diameter. As the number of layers progresses, the difference increases and stubbing occurs [21,35], generating unstable deposition conditions. Within the stable conditions, the deposits show good geometrical accuracy. Porosity is observed to a very limited extent with the presence of round pores. Such pore formation is expected to be due to the entrapment of metallic vapour or the process gas during the process [14].

In the light of the results, further metallurgical characterization was carried out on multi-layered deposits with 21 layers obtained using 220 μm height increment.

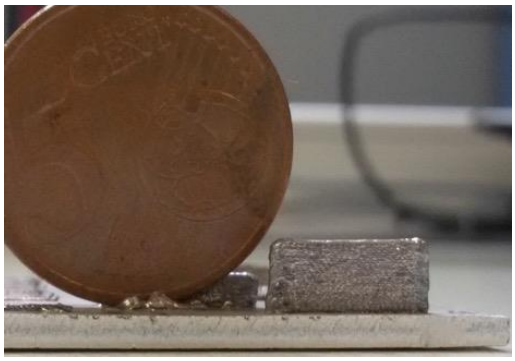

Figure 4. Example of a manufactured thin wall showing high quality conditions next to a 5 Euro cent coin for dimensional comparison.

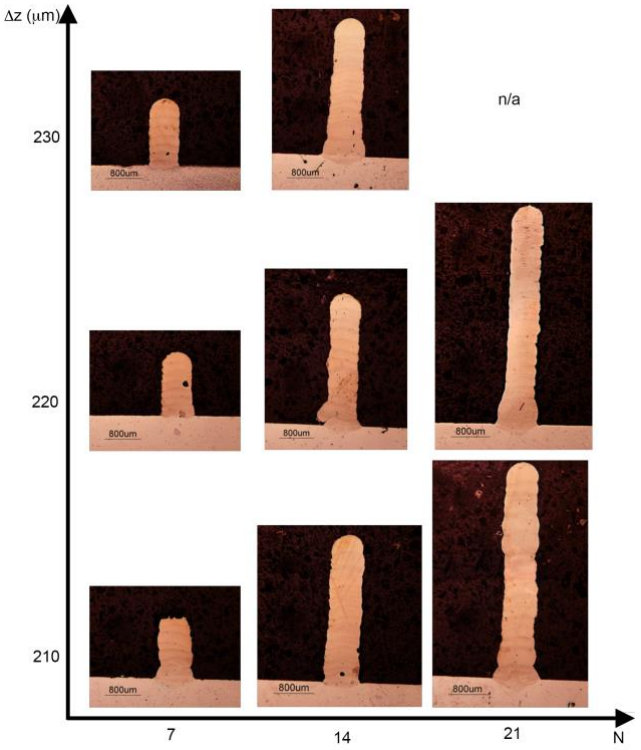

Figure 5. Cross-section images of the multi-layered depositions as a function of height increment (Δz) and layer number (N).

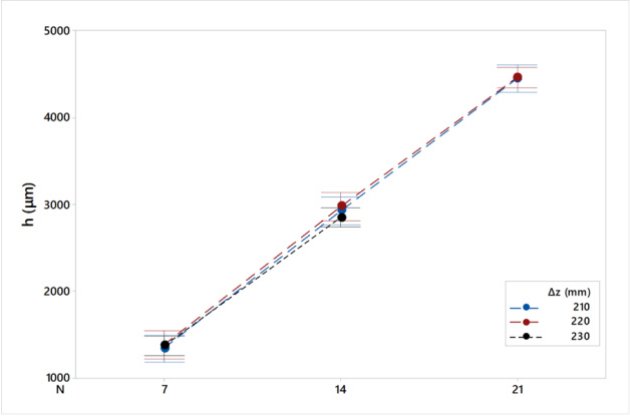

Figure 6. Height (*h*) of the multi-layered depositions as a function of height increment (Δz) and layer number (*N*).

3.3. Macroscale characterization of the multilayered deposit: compositional and microhardness analyses

A macroscale characterization in terms of chemical composition and microhardness analyses is required to assess the integrity and uniformity of the deposited structures in the view of their use in final applications. In Figure 7.a the cross section of a multi-layered part, acquired by SEM using secondary electron signal, is depicted. No defects, such as cracks or pores, can be seen in the multi-layered deposition. The compositional analysis was carried out along the entire height of the deposited part, in separate areas depicted by the rectangles in Figure 7a. Figure 7b shows the compositional profile of the principal elements, namely Al, Si

and Mg, expressed in weight percentage, ranging from the upper layer (area 1) down to the 5754 base plate (area 12).

The multi-layered deposition has a uniform chemical composition ($Al_{85}Si_{15}$ in % wt.) along the build direction until the base plate intermixing zone (areas 1 to 9). On the contrary, around the base plate-deposit interface (area 10) Mg appear to be present in a small amount and the Si content decreases significantly. The Mg gain is due to the base plate, as the initial wire does not show any traces of this element (see EDS profile of the wire in Figure 7b). The reduction in the Si content in the intermixing zone is due to the dilution with the 5754 base plate, which is Si free.

The compositional trend of Figure 7.b indicates that the intermixing zone starts from the initial few hundreds of microns in the multi-layered wall and extends within the base plate (area 10-11-12). Therefore, the mechanical properties of the deposition can be linked to both the chemical composition, and the microstructure induced by the high cooling rate present during the laser deposition. Figure 7.c reports the profile of Vickers micro-hardness values. The micro-hardness of the multilayered deposit is around 120 HV with a relatively constant profile up to the top part of the deposit. Evidently, the last deposited layers, shows a higher micro-hardness up to 130 HV. The absence of a successive layer prevents a consecutive heat cycle applied to the already deposited layer acting as an annealing step.

Another microhardness variation was detected in the intermixing region corresponding to the areas 10-11-12 of Figure 7a. This behavior can be linked to mechanical properties of parts, processed using different manufacturing routes (i.*e.* hot and cold rolled base plate, laser deposited wire) and consequently different microstructures and different chemical compositions. Compared to the microhardness of the initial wire (approximately 50 HV) and the Al-Mg base plate (approximately 70 HV), the multilayered deposit of the Al-Si alloy shows a much higher hardness (approximately 120 HV). The obtained hardness is comparable to electron beam deposited 2139 alloy wires after a consecutive aging treatment of more than 20 hours [31]. Similar hardness values through the SLM process performed on similar alloy (i.e. AlSi10Mg) using a PW laser was achieved, presumably due to equivalent cooling rates [36].

It can be noted that the fast cooling cycles induced by the µLMWD process can improve the mechanical properties of the Al-alloy. The good weldability of the wire material combined with the correct selection of the process parameters provides a stable process free of cracks or delamination from the base plate. Such

features can be exploitable especially for the use of depositing fine features to existing components. Fine ribs with high mechanical strength can be used in a hybrid manufacturing scheme, adding value to the component by providing fine structures hard to achieve by conventional manufacturing processes. In a similar way, the process can be used to tailor the mechanical properties of the part by adding harder features on a specific location of the component.

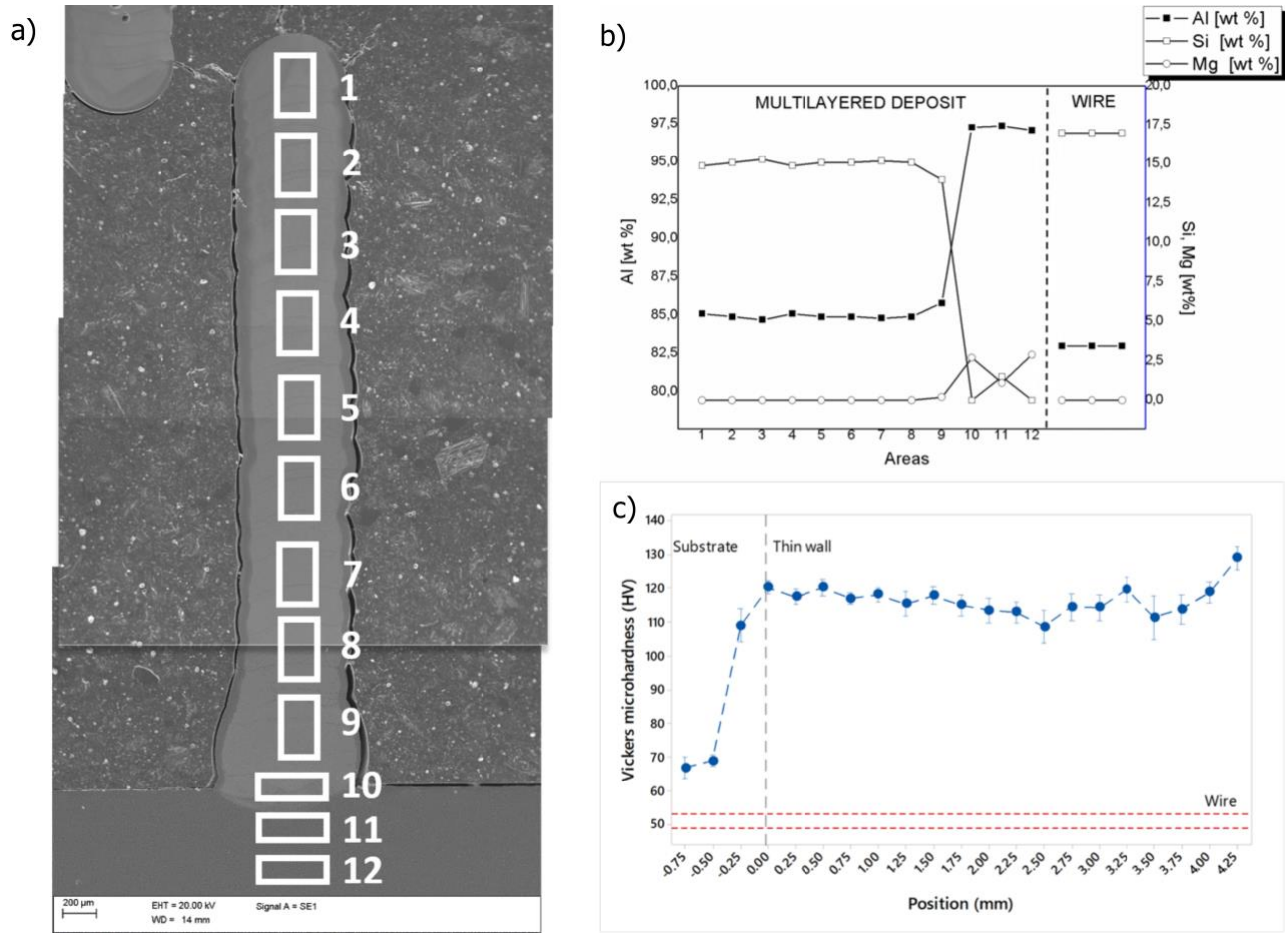

Figure 7. SEM image of the multi-layered deposition, containing the areas where EDS measurements were performed (a) and corresponding compositional profile (b); microhardness profile of the multi-layered deposition, where error bars represent standard error (c).

3.4. Microscale characterization of the multi-layered deposit: microstructural analysis of the deposit and mixing zone

A microscale characterization is required for a better comprehension on how the process affects the material properties. The overall observations showed that layer-by-layer building strategy does produce discontinuities in the microstructure. A very fine microstructure, coming from a rapid and directional cooling, well known

characteristics of laser fusion processing is present, as seen in Figure 8.a. Along the build direction within the stable microhardness region a homogenous microstructure was observed. The microstructure was found to remain homogenous also on the horizontal axis. Powder based DED processes commonly have microstructural variations on both build direction and the horizontal axis [9]. A similar microstructural variation appears also on Ti6Al4V processed by wire-based macro DED processes using laser and electric arcs as the heat source [37]. The main difference of the µLMWD process is the use of a relatively more homogenous heat source. Essentially the laser beam is larger than the feedstock material, and the use of pulsed wave emission provides the means for excessive heat build-up. Hence, a more homogenous temperature field is retained during the process.

Figure 8.a shows the overlapping among a deposited layer and the previous one. The border among two layers shows a microstructural modification within the extent of approximately 10 µm. The generation of this band is expected to be due to the annealing effect of the successive layer on the previous one. Figure 8.b shows a magnified image of the highlighted zone in Figure 8.a. The observed band consists in a thin region, in which Al and Si dispersion is modified. The microstructure obtained shows a continuous network of Si dispersed into the matrix of Al. The thin Si network affirms that the cooling rates during laser deposition are very rapid, such as those occurring in SLM process [36]. On the contrary, soaking for longer times at temperatures able to induce any microstructural modifications in the material can provoke a different morphology of the Si phase.

Figure 8.b indicates the presence of four different microstructure types across the single border of the heat affected zone (HAZ). Zone 1, representative of the microstructure obtained within the single layer, has an equiaxial distribution of Si network, indicating no preferential direction of cooling but a uniform orientation. Below this, zone 2 represents the Si phase elongated along the cooling orientated parallel to the build direction, where the Si network remains continuous. In zone 3 the Si network starts to be broken and in zone 4 the thinner network is visible, having partially fractured sub-micrometric islands of Si. Evidently, between successive layers a dilution zone is present, undergoing to a second heating cycle, which can cause the rupture of the fine Si network, acting as a local heat treatment. The generation of such separate and small Si islands was observed when SLM built AlSi10Mg samples were annealed at temperatures higher than the one detected by the transformation peaks [36]. This confirms that the line, depicted in Figure 8.a, is associated to the region where

the critical temperature is overcome with the given heat flux, reorganizing the microstructure of the previously melted layer.

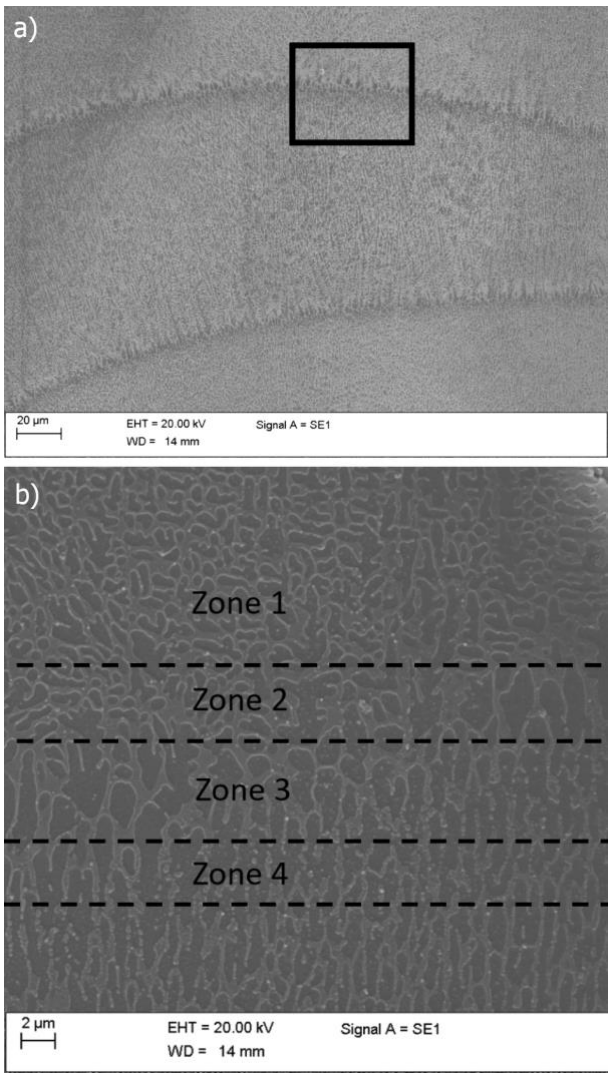

Figure 8. SEM image of the overlapping zone between successive layers (a), a magnification of region bordered by the black rectangle of the previous image (b).

As reference, the microstructure of the cold-drawn and annealed feedstock wire, shows globular and separate islands of Si (see Figure 9). The size of the Si spheres ranges between 1 to 5 µm and is much larger than the Si network found in the multi-layered deposit, which is thinner than 1 µm. These differences in microstructure can well explain the mechanical properties, microhardness at first.

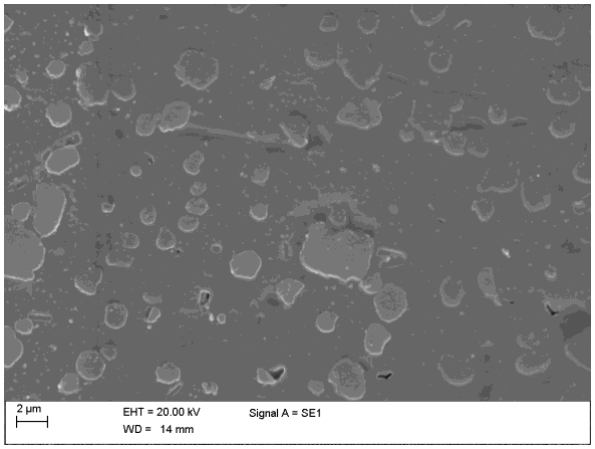

Figure 9. Microstructure of the wire feedstock.

Moreover, different microstructures and compositions can be found in proximity of the base plate. This part can be seen crucial in the view of laser deposition on existing components, while it can be seen like a support in the view of an additive manufacturing free-standing components, where the printed part has to be removed from the building platform. Starting from the compositional profile depicted in Figure 7.b, the interphase region has been investigated at higher magnification. The punctual measurements of chemical composition were performed via EDS, as shown in Figure **10**.a, for obtaining the content profile of the principal elements. The compositional evolution is depicted in Figure **10**.b. The Al and Mg contents increase from the base of the multi-layered deposit down to the base plate from 85 wt % to 97 wt % and from 0 wt % to 3 wt %, respectively. The Si content drops down from 14 wt % to 0 wt%. These profiles are in good agreement with the chemical composition of both initial wire and base plate and no element lost was detected. However, these compositional gradients suggest the presence of a mixing area, in which an exchange of elements between the deposit and the base plate is present.

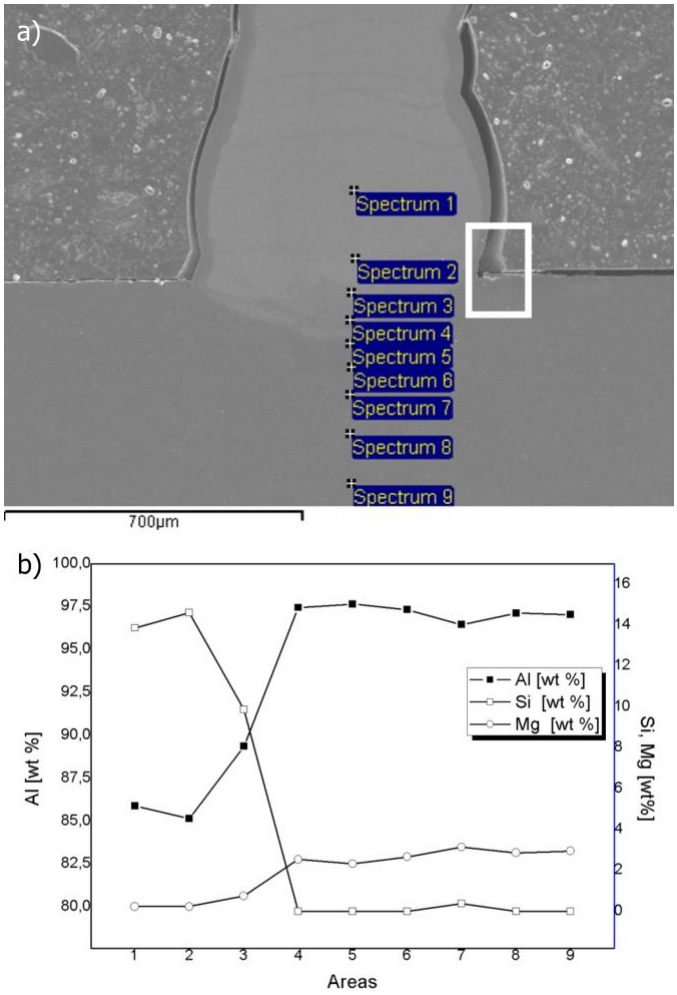

Figure 10. SEM image of the contact area between the thin-wall deposit and the base plate, showing EDS measurement points (a), distribution of the alloying elements (b).

Further chemical composition analysis was concentrated in a lateral portion of the latter zone, indicated by the white rectangle highlighted in Figure 10.a. In Figure 11.a and b magnification of the area of interest and corresponding compositional profile are shown, respectively. Figure 11.a highlights a limited dilution ratio among the two Al alloys. In the upper part on the left of the picture the microstructure of the deposit is orientated following different directions, as previously discussed. In particular, the Si network is vertically elongated. The base plate has the function of heat sink and it can offer a directional cooling. The arrows in Figure 11.a represents the direction of the heat flow (q''), viewed as elongation direction of the grains.

Another intriguing feature of the mixing zone is the shape of the border between the microstructural and compositional change. As shown with the dashed curve in Figure 11a, the fine Si-network of the thin-wall deposit does not extend completely to down the base plate. This curved profile is due to mixing of the two aluminium alloys in liquid state, occurring during the first laser deposition penetrating into the first layer. This phenomenon is confined in a very thin extent, which values approximately few tenths of microns. Moreover,

the material exchange appears to depend on the position. The base plate alloy appears to mix into the deposit around the borders (arrow indicating *), whereas the wire alloy penetrates inside the base plate in the central portion of the dilution area (arrow indicating **). Figure 11.b shows the compositional profile, obtained in four white areas of Figure 11.a. The compositional profiles confirm the presence of the mixing area, placed along the dotted black curve of Figure 11.a. The Al content increases moving from the deposit down to the base plate, being 5754 alloy richer of Al than the 4047 one. Similar trend is seen for Mg, while a reduction of Si content has been detected.

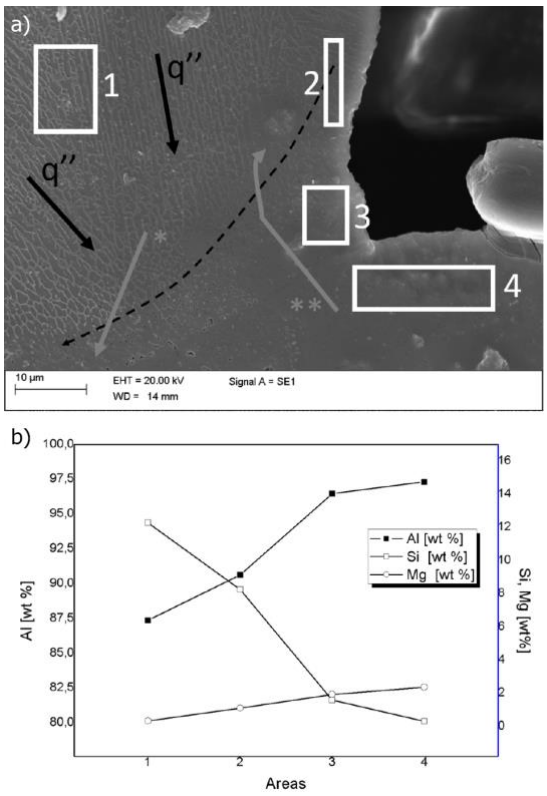

Figure 11. SEM magnification of the lateral part of the interface among deposit and platform, highlighting four areas for EDS analysis; compositional profile (b).

4. Conclusions

This work reports the use of µLMWD to deposit 4047 Al-alloy for producing multi-layered thin-walled components. The paper discusses the processing condition required for a stable deposition and the metallurgical properties of the obtained deposits . The main conclusions are as follows.

- The single-layer deposition of the thin Al-alloy wire is characterized by a narrow process window, in which a large thickness variation could be observed. This confirms the sensitivity of the material to the energy input due to the high reflectivity and low melting point.
- In multiple-layer deposits, the process stability highly relies on the height increment applied. The height increment should be suitably lower than the single layer height (approximately 90% of the single layer height) to accommodate correct dilution between layers. At stable conditions, the multi-layered deposits are pore and crack-free.
- The microhardness profile of the multi-layered deposits show approximately 140% increase in microhardness compared to the wire feedstock. Compared to the cold-rolled base plate material of a more complex alloy, the microhardness is approximately 70% higher. Moreover, a homogenous microhardness along the build direction is observed a slight increase at the final layer.
- The microstructure of the thin-walled deposit shows a very thin Si-network, while the chemical composition is maintained. The microstructure is homogenous also along the build direction. Such features prove that the μLMWD process can be effective in managing the heat input and limit the multiple annealing of previous layers.
- The compositional analysis shows that at the mixture zone the deposit and base plate exchange elements in preferential zones. Moreover, due to the heat flow the microstructure changes following the direction of the heat towards the base plate.

The process proves to be a valid option for providing added features with graded mechanical properties on existing components. Such improved properties can be achieved even with the use of a modest Al-alloys destined to be used as a filler materials. For producing free-standing components, the high precision appears as an appealing option as a compromise between powder bed fusion and macro DED processes. Further studies on the heat treatment are required, which should assess the possibility to apply any stress-relieving stages, which might be required to avoid dimensional inaccuracies upon the detachment of the part from the base plate.

Acknowledgements

The authors wish to express their gratitude to Daniele Rocchitelli and Eligio Grossi for their contribution to the system development and experimental work. This work was supported by European Union, Repubblica Italiana, Regione Lombardia and FESR for the project MADE4LO under the call "POR FESR 2014-2020 ASSE I - AZIONE I.1.B.1.3".

References

[1] Wong M, Tsopanos S, Sutcliffe CJ, Owen I. Selective laser melting of heat transfer devices. Rapid Prototyp J 2007;13:291–7. doi:10.1108/13552540710824797.

[2] Wong M, Owen I, Sutcliffe CJ, Puri A. Convective heat transfer and pressure losses across novel heat sinks fabricated by Selective Laser Melting. Int J Heat Mass Transf 2009;52:281–8. doi:10.1016/j.ijheatmasstransfer.2008.06.002.

[3] Maskery I, Aremu AO, Simonelli M, Tuck C, Wildman RD, Ashcroft IA, et al. Mechanical Properties of Ti-6Al-4V Selectively Laser Melted Parts with Body-Centred-Cubic Lattices of Varying cell size. Exp Mech 2015:1–12. doi:10.1007/s11340-015-0021-5.

[4] Steen WM, Mazumder J. Laser Material Processing. London: Springer London; 2010. doi:10.1007/978-1-84996-062-5.

[5] Dinda GP, Dasgupta AK, Bhattacharya S, Natu H, Dutta B, Mazumder J. Microstructural Characterization of Laser-Deposited Al 4047 Alloy. Metall Mater Trans A 2013;44:2233–42. doi:10.1007/s11661-012-1560-3.

[6] Ding Y, Muñiz-Lerma JA, Trask M, Chou S, Walker A, Brochu M. Microstructure and mechanical property considerations in additive manufacturing of aluminum alloys. MRS Bull 2016;41:745–51. doi:10.1557/mrs.2016.214.

[7] Akinlabi ET, Akinlabi SA. Advanced Coating : Laser Metal Deposition of Aluminium Powder on Titanium Substrate. Proc. World Congr. Eng. 2016, vol. II, 2016, p. 1–6.

[8] Caiazzo F, Alfieri V, Argenio P, Sergi V. Additive manufacturing by means of laser-aided directed metal deposition of 2024 aluminium powder: Investigation and optimization. Adv Mech Eng 2017;9:168781401771498. doi:10.1177/1687814017714982.

[9] Javidani M, Arreguin-Zavala J, Danovitch J, Tian Y, Brochu M. Additive Manufacturing of AlSi10Mg Alloy Using Direct Energy Deposition: Microstructure and Hardness Characterization. J Therm Spray Technol 2017;26:587–97. doi:10.1007/s11666-016-0495-4.

[10] Singh A, Ramakrishnan A, Baker D, Biswas A, Dinda GP. Laser metal deposition of nickel coated Al 7050 alloy. J Alloys Compd 2017;719:151–8. doi:10.1016/j.jallcom.2017.05.171.

[11] Thompson SM, Bian L, Shamsaei N, Yadollahi A. An overview of Direct Laser Deposition for additive manufacturing; Part I: Transport phenomena, modeling and diagnostics. Addit Manuf 2015. doi:10.1016/j.addma.2015.07.001.

[12] Dutta B, Froes FH (Sam). The Additive Manufacturing (AM) of titanium alloys. Met Powder Rep 2017;72:96–106. doi:10.1016/j.mprp.2016.12.062.

[13] Louvis E, Fox P, Sutcliffe CJ. Selective laser melting of aluminium components. J Mater Process Technol 2011;211:275–84. doi:10.1016/j.jmatprotec.2010.09.019.

[14] Weingarten C, Buchbinder D, Pirch N, Meiners W, Wissenbach K, Poprawe R. Formation and reduction of hydrogen porosity during selective laser melting of AlSi10Mg. J Mater Process Technol 2015;221:112–20. doi:10.1016/j.jmatprotec.2015.02.013.

[15] Lincoln Electric. Aluminum MIG and TIG Products n.d. https://www.lincolnelectric.com/en-ca/consumables/aluminum-mig-tig/Pages/aluminum-mig-tig.aspx (accessed July 23, 2018).

[16] AlcoTechnics. Aluminum Mig (GMAW) Welding Wire n.d. http://www.alcotec.com/us/en/products/aluminum-mig-welding-wire.cfm (accessed July 23, 2018).

[17] Syed WUH, Pinkerton AJ, Li L. A comparative study of wire feeding and powder feeding in direct

diode laser deposition for rapid prototyping. Appl Surf Sci 2005;247:268–76. doi:10.1016/j.apsusc.2005.01.138.

[18] Brandl E, Baufeld B, Leyens C, Gault R. Additive manufactured Ti-6A1-4V using welding wire: Comparison of laser and arc beam deposition and evaluation with respect to aerospace material specifications. Phys Procedia 2010;5:595–606. doi:10.1016/j.phpro.2010.08.087.

[19] Martina F, Mehnen J, Williams SW, Colegrove P, Wang F. Investigation of the benefits of plasma deposition for the additive layer manufacture of Ti-6Al-4V. J Mater Process Technol 2012;212:1377–86. doi:10.1016/j.jmatprotec.2012.02.002.

[20] Ghosh PK, Goyal VK, Dhiman HK, Kumar M. Thermal and metal transfer behaviours in pulsed current gas metal arc weld deposition of Al–Mg alloy. Sci Technol Weld Join 2006;11:232–42. doi:10.1179/174329306X89251.

[21] Motta M, Demir AG, Previtali B. High-speed imaging and process characterization of coaxial laser metal wire deposition. Addit Manuf 2018;22:497–507. doi:10.1016/j.addma.2018.05.043.

[22] Ding D, Pan Z, Cuiuri D, Li H. Wire-feed additive manufacturing of metal components: technologies, developments and future interests. Int J Adv Manuf Technol 2015;81:465–81. doi:10.1007/s00170-015-7077-3.

[23] Kim JD, Kang KH, Kim JN. Nd : YAG laser cladding of marine propeller with hastelloy C-22. Appl Phys A 2004;79:1583–5. doi:10.1007/s00339-004-2854-0.

[24] Kim J Do, Peng Y. Plunging method for Nd:YAG laser cladding with wire feeding. Opt Lasers Eng 2000;33:299–309. doi:10.1016/S0143-8166(00)00046-4.

[25] Hussein NIS, Segal J, McCartney DG, Pashby IR. Microstructure formation in Waspaloy multilayer builds following direct metal deposition with laser and wire. Mater Sci Eng A 2008;497:260–9. doi:10.1016/j.msea.2008.07.021.

[26] Demir AG. Micro laser metal wire deposition for additive manufacturing of thin-walled structures. Opt Lasers Eng 2018;100. doi:10.1016/j.optlaseng.2017.07.003.

[27] Vaezi M, Seitz H, Yang S. A review on 3D micro-additive manufacturing technologies. Int J Adv Manuf Technol 2013;67:1721–54. doi:10.1007/s00170-012-4605-2.

[28] Demir AG, Previtali B. Additive manufacturing of cardiovascular CoCr stents by selective laser melting. Mater Des 2017;119. doi:10.1016/j.matdes.2017.01.091.

[29] Williams SW, Martina F, Addison AC, Ding J, Pardal G, Colegrove P. Wire + Arc Additive Manufacturing. Mater Sci Technol 2016;32:641–7. doi:10.1179/1743284715Y.0000000073.

[30] Shen C, Pan Z, Ma Y, Cuiuri D, Li H. Fabrication of iron-rich Fe-Al intermetallics using the wire-arc additive manufacturing process. Addit Manuf 2015;7:20–6. doi:10.1016/j.addma.2015.06.001.

[31] Brice C, Shenoy R, Kral M, Buchannan K. Precipitation behavior of aluminum alloy 2139 fabricated using additive manufacturing. Mater Sci Eng A 2015;648:9–14. doi:10.1016/j.msea.2015.08.088.

[32] Horgar A, Fostervoll H, Nyhus B, Ren X, Eriksson M, Akselsen OM. Additive manufacturing using WAAM with AA5183 wire. J Mater Process Technol 2018;259:68–74. doi:10.1016/j.jmatprotec.2018.04.014.

[33] Cao X, Wallace W, Poon C, Immarigeon JP. Research and progress in laser welding of wrought aluminum alloys. I. Laser welding processes. Mater Manuf Process 2003;18:1–22. doi:10.1081/AMP-120017586.

[34] Cayless RBC. Alloy and Temper Designation Systems for Aluminum and Aluminum Alloys. ASM

Handbook, Vol. 2. Online, ASM International; 1990, p. 15–28.

[35] Abioye TE, Folkes J, Clare AT. A parametric study of Inconel 625 wire laser deposition. J Mater Process Technol 2013;213:2145–51. doi:10.1016/j.jmatprotec.2013.06.007.

[36] Fiocchi J, Tuissi A, Bassani P, Biffi CA. Low temperature annealing dedicated to AlSi10Mg selective laser melting products. J Alloys Compd 2017;695:3402–9. doi:10.1016/j.jallcom.2016.12.019.

[37] Baufeld B, Brandl E, Van Der Biest O. Wire based additive layer manufacturing: Comparison of microstructure and mechanical properties of Ti-6Al-4V components fabricated by laser-beam deposition and shaped metal deposition. J Mater Process Technol 2011;211:1146–58. doi:10.1016/j.jmatprotec.2011.01.018.

List of figures

Figure 1. Details of the μWLMD system. a) Overview of the welding station and the laser source. b) CAD model of Lachesis wire feeder. c) Close up image of the deposition zone showing the wire feed and deposition direction.

Figure 2. Cross-section images of the single-layer depositions as function of process parameters.

Figure 3. Single track width (w) as a function of pulse duration (τ) and energy (E). Error bars represent standard error.

Figure 4. Example of a manufactured thin wall showing high quality conditions next to a 5 Euro cent coin for dimensional comparison.

Figure 5. Cross-section images of the multi-layered depositions as a function of height increment (Δz) and layer number (N).

Figure 6. Height (h) of the multi-layered depositions as a function of height increment (Δz) and layer number (N).

Figure 7. SEM image of the multi-layered deposition, containing the areas where EDS measurements were performed (a) and corresponding compositional profile (b); microhardness profile of the multi-layered deposition, where error bars represent standard error (c).

Figure 8. SEM image of the overlapping zone between successive layers (a), a magnification of region bordered by the black rectangle of the previous image (b).

Figure 9. Microstructure of the wire feedstock.

Figure 10. SEM image of the contact area between the thin-wall deposit and the base plate, showing EDS measurement points (a), distribution of the alloying elements (b).

Figure 11. SEM magnification of the lateral part of the interface among deposit and platform, highlighting four areas for EDS analysis; compositional profile (b).

List of tables

Table 1. Nominal chemical composition of the wire and base plate materials [34].

Table 2. Fixed and varied parameters in the study of single-layer depositions experiments.

Table 3. Fixed and varied parameters in the study of multi-layer depositions experiments.

Table 4. ANOVA table for single track width (w).